AIAA 99–2424

Laser Induced Fluorescence Measurement of Ion Velocities in the Plume of a Hall Effect Thruster

George J. Williams, Jr., Timothy B. Smith,
Frank S. Gulczinski, III, Brian E. Beal,
Alec D. Gallimore, and R. Paul Drake
University of Michigan, Ann Arbor, MI 48109

35th AIAA/ASME/SAE/ASEE Joint Propulsion Conference and Exhibit
20–23 June 1999/Los Angeles, CA

Laser Induced Fluorescence Measurement of Ion Velocities in the Plume of a Hall Effect Thruster

George J. Williams, Jr.,* Timothy B. Smith,*
Frank S. Gulczinski, III,* Brian E. Beal,†
Alec D. Gallimore,‡ and R. Paul Drake§
University of Michigan, Ann Arbor, MI 48109

Laser induced fluorescence (LIF) was used to measure the mean and variance of the velocity distribution of xenon ions in the plume of the P5 Hall thruster. The data indicate an acceleration region extending several centimeters downstream of the exit plane. Significant plume divergence and spreads in velocities equivalent to about 1 eV were observed. Speeds measured correspond to ion energies smaller than those measured with molecular beam spectroscopy at similar points of interrogation in the plume. LIF measurements taken 10 to 50 cm downstream indicate that the "spike" observed in the plume is a region of interaction caused by inward divergence from the discharge annulus.

A	Nuclear magnetic dipole interaction constant
B	Nuclear electric quadrapole interaction constant
c	Light speed, 2.9979×10^8 m/s
E	Term energy, J
F	Total angular momentum quantum number
$g(\nu)$	Thermally-broadened lineshape
h	Planck constant, 6.6261×10^{-34} J-s
I	Nuclear spin quantum number
I_{sp}	Specific impulse, s
J	Electronic angular momentum quantum number
k	Boltzmann constant, J/K
M	Ion mass, kg
T	Temperature, K
v	Velocity component, m/s
α	Downstream beam angle from vertical, deg
β	Lateral beam angle from vertical, deg
ν	Frequency, Hz

Subscripts

A	Axial
D	Downstream
hfs	Hyperfine structure
is	Isotopic structure
O	Off-axis
o	Line center
R	Radial

*Graduate Student, Student Member, AIAA.
†Undergraduate Student, Student Member, AIAA.
‡Associate Professor and director of lab, Associate Fellow AIAA.
§Professor.

Introduction

ELECTRIC propulsion devices such as ion engines and Hall thrusters are emerging as replacements for chemical rockets on satellites and planetary probes; their higher specific impulse allows them to use significantly less propellant. Accurate measurements of thruster performance and predictions of spacecraft contamination are crucial for their application.

The ion energy distributions in the plumes of Hall thrusters have been the object of extensive diagnostic investigations. Retarding potential analyzers (RPAs),[1] laser induced fluorescence (LIF),[2] molecular beam mass spectroscopy (MBMS)[1,3] and various other probes[4] have been used to evaluate the performance of thrusters and their integration on spacecraft. However, probes may perturb the plasma, yielding data that are not representative of the actual thruster performance.

Differences in these measurements may be due to the accuracy of the measurement, to differences in the ion energy characteristics at different downstream positions in the plume, or to a combination of these and other factors.

LIF measurements were performed from 0.01 to 0.5 m downstream of the exit plane of a Hall thruster to generate near-field and some far-field data to compare to probe (MBMS) data. All experiments were performed in the large vacuum test facility (LVTF) at the Plasmadynamics and Electric Propulsion Laboratory (PEPL) at the University of Michigan.

Theory

Laser Induced Fluorescence

Laser induced fluorescence (LIF) is the incoherent emission of photons from an unstable energy level

(electronic in the case of xenon or other monatomics) populated by the absorption of photons from the laser. In general, the wavelengths (*i.e.*, energies) of the absorbed and emitted photons are different. Indeed, emission may occur at many different wavelengths.

The absorbing singly ionized xenon, Xe II, will "see" the wavelength of the incoming photons shifted by the relative motion of the ion in the direction of the photon. This Doppler effect is observed as a shift in the resonant wavelength as the laser is scanned over a very short range. The change in photon frequency $\triangle\nu$ is

$$\triangle\nu = \nu_o v_i/c = v_i/c \tag{1}$$

Xe II has natural absorption/emission transitions throughout the visible spectrum. The $5d^4D - 6p^4P^0$ (605.28 nm) Xe II transition was selected to stimulate the emission. The $6s^4P - 5p^4P^0$ (529 nm) emission is strongest for this upper state and was selected to be collected.

Both two-beam and three-beam configurations interrogated the plasma. Two beams permitted simultaneous measurements of azimuthal and axial velocity components.[5] Three beams yielded simultaneous azimuthal, axial, and radial velocity components.

The beams were split just downstream of the dye laser, as shown in Fig. 1. The beams entered the chamber parallel to each other, were reflected downward and passed through a focusing lens, crossing at the focal point of the lens–the LIF interrogation point. The lens also reduced the beam diameters (which had grown over the 12 m path length) to less than 0.1 cm.

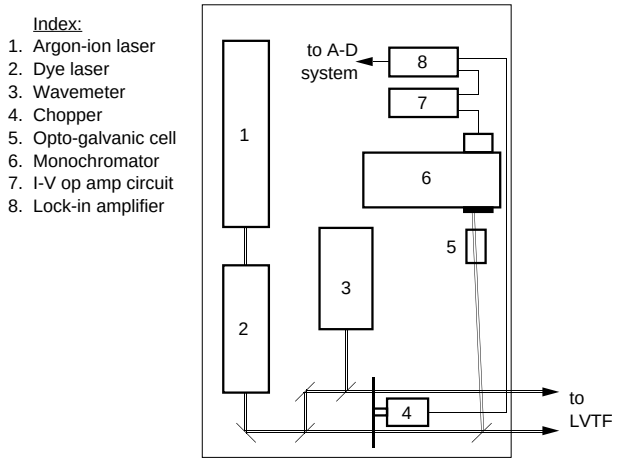

Fig. 1 Laser division and modulation.

The beam passing through the focusing lens center remained perpendicular to the axis of the thruster, directly measuring the azimuthal component of velocity, and is referred to below as the "vertical" beam. A second beam, referred to as the "downstream" beam, entered the focusing lens downstream from the lens center, measuring the velocity at an angle α from vertical and perpendicular to the thruster face. The third beam, the "lateral," entered the focusing lens at the third vertex of a right triangle, measures the velocity at an angle β from vertical and parallel to the thruster face. Figure 2 shows the relationships between measured and calculated velocities.

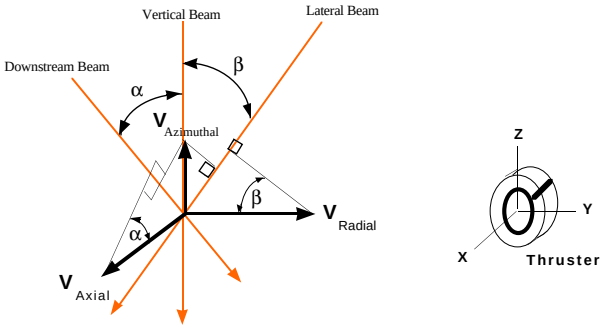

Fig. 2 Measured and calculated velocities.

The axial velocity component v_A can be deduced from the vertical velocity v_V and the downstream velocity v_D by

$$v_A = \frac{v_D - v_V \cos\alpha}{\sin\alpha} \tag{2}$$

Similarly, the lateral velocity v_L and v_V yield the radial velocity

$$v_R = \frac{v_L - v_V \cos\beta}{\sin\beta} \tag{3}$$

Assuming statistical independence of the temperatures (distributions) associated with each velocity component, the true axial temperature, T_A, can be calculated given the "temperatures" in the radial, T_R, and off-axis, T_O, directions. This assumption yields an elliptical relationship:

$$\cos^2(\pi/2-\alpha) + (T_V/T_A)^2 \sin^2(\pi/2-\alpha) = (T_V/T_O)^2 \tag{4}$$

Solving for the axial temperature yields

$$T_A = T_V \left[\frac{(T_V/T_O)^2 - 1}{\cos^2\alpha} + 1\right]^{-1/2} \tag{5}$$

Similarly, T_R is a function of T_L, T_V, and β:

$$T_R = T_V \left[\frac{(T_V/T_L)^2 - 1}{\cos^2\beta} + 1\right]^{-1/2} \tag{6}$$

Fluorescence Lineshape Model

There are nine stable isotopes of xenon, seven of which have natural abundances greater than one percent. Each of these isotopes has a slightly different term energy at a given energy level. This energy difference results in isotopic splitting.

The two isotopes with an odd atomic mass, ^{129}Xe and ^{131}Xe, have a non-zero nuclear spin quantum number I, resulting in hyperfine splitting of the atomic energy levels. This hyperfine structure (hfs) is considerably broader than the isotopic structure, and provides most of this transition's characteristic shape.

The lighter isotope, ^{129}Xe, has $I = 1/2$, while ^{131}Xe has $I = 7/2$. The total angular momentum quantum number F takes values

$$F = I + J, I + J - 1, \ldots, |I - J| \tag{7}$$

where J is the total electronic angular momentum.[6] Figure 3 shows the hyperfine splitting and allowed transitions for the $^4P_{5/2} - ^4D_{7/2}$ line.

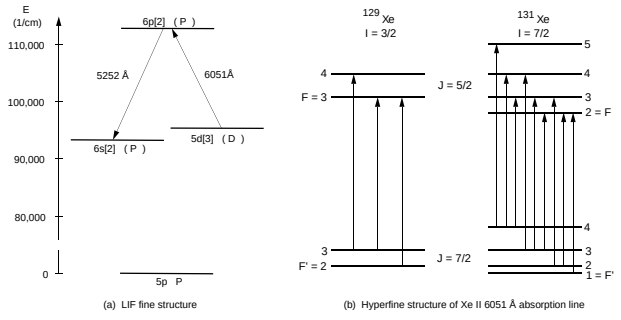

Fig. 3 Hyperfine structure of Xe II.

The extra term energy due to hfs is given by

$$E_{hfs} = A\frac{C}{2} + B\frac{(3C/4)(C+1) - I(I+1)J(J+1)}{2I(2I-1)J(2J-1)} \tag{8}$$

where A is the nuclear magnetic dipole interaction constant, B is the nuclear electric quadrapole interaction constant and

$$C = F(F+1) - I(I+1) - J(J+1) \tag{9}$$

The transition rule for hyperfine splitting is of a familiar form, $\triangle F = 0, \pm 1$ where $F = 0 \rightarrow F' = 0$. The relative intensity of each hyperfine component is given for a $J \rightarrow J - 1$ transition by[7]

$$I(F \rightarrow F-1) \propto \frac{P(F)P(F-1)}{F} \tag{10}$$

$$I(F \rightarrow F) \propto \frac{(2F+1)}{F(F+1)}P(F)Q(F) \tag{11}$$

$$I(F-1 \rightarrow F) \propto \frac{Q(F)Q(F-1)}{F} \tag{12}$$

where $P(F) = (F+J)(F+J+1) - I(I+1)$ and $Q(F) = I(I+1) - (F-J)(F-J+1)$.

This model uses published isotopic shifts and hyperfine structure constants for the Xe II $^4P_{5/2}$ and $^4D_{7/2}$ energy levels.[8]

To properly model line broadening, we would normally convolve instrument and thermal broadening into a Voigt profile.[9] In classical emission and absorption spectroscopy, the relevant Lorentzian linewidth belongs to the monochromator; for LIF, though, the monochromator remains at a constant setting, simply acting as a line filter, and the relevant Lorentzian linewidth belongs to the laser.

For plasmas at or above room temperature, the laser linewidth $\nu_L \approx 1$ MHz is much smaller than the Doppler broadening ν_D , and the Voigt profile simplifies to a purely thermally-broadened lineshape

$$g(\nu) = \frac{1}{\nu_o}\left(\frac{\tau}{\pi}\right)^{1/2} \exp\left(-\tau\left[\frac{\nu - \nu_o}{\nu_o}\right]^2\right) \tag{13}$$

where $\tau = Mc^2/2kT$.

For the isotopes with even mass numbers (i.e., without hfs), the line intensity is linearly proportional to the naturally-occurring abundance for each isotope. For ^{129}Xe and ^{131}Xe, the line intensity is linearly proportional to the product of the isotopic abundance and the relative intensity of the hyperfine components. Thus, the signal resulting from scanning the laser over the absorption wavelength range is the sum of $N = 17$ lines,

$$S(\nu) = C\sum_{i=1}^{N} p_i g_i(\nu) \tag{14}$$

where p_i is the intensity for each line i, $g_i(\nu)$ is the shape function given above and C is a constant representing a whole series of unknowns, including plasma density, collection solid angle, monochromator throughput, photomultiplier tube efficiency, output current-to-voltage amplification and analog-to-digital converter range. The center for each line is

$$\nu_i = [(E + E_{hfs} + E_{is})' - (E + E_{hfs} + E_{is})'']/h, \tag{15}$$

where E_{hfs} is the hyperfine term energy and E_{is} is the isotopic shift.[8]

By varying the temperature T and frequency shift with respect to a stationary reference plasma $\triangle\nu$, the modeled signal can provide a good fit to the data. An IDL code implementing this model was developed, using a Davidson-Fletcher-Powell optimization routine to provide a replicable "best-fit."

Apparatus and Procedure

Thruster

The University of Michigan, in conjunction with the United States Air Force, has developed a 5 kW class Hall thruster, the P5, for basic research purposes. A photograph of the thruster is given in Fig. 4. This thruster underwent performance and probe testing[10] that indicated it operated at performance levels and in a manner consistent with thrusters under commercial development.[11–13]

Thruster power was provided by laboratory power supplies. The main discharge was supplied by a Sorensen Model DCR 600-16T. The electromagnets were powered separately, the inner by a Kikusui Model PAD 55-10L and the outer by a Kikusui Model PAD 35-10L. The cathode heater was a Sorensen Model DCS 55-55, and the igniter was a custom-built high-voltage ignition supply. The thruster discharge circuit was electrically isolated during operations. A filter

Fig. 4 Photograph of the P5 Hall effect thruster.

consisting of 1.3 Ω equivalent resistance in series with the discharge current and a 95 μF capacitor in parallel was used to damp out thruster oscillations.

The annular discharge channel is 2.5 cm wide and is on a 7.4 cm radius. The cathode was mounted at roughly 45 degrees from vertical to facilitate LIF. The P5 was interrogated at 0, ±0.5 and ±1.0 cm from the center of the discharge channel. The P5 was moved axially to enable interrogation from 0.1 to 50 cm. Table 1 gives the thruster operating conditions used in this study.

Facility

Tests were performed in the 6 m x 9 m LVTF. This is the same facility used in previous work at PEPL, but prior to these tests, it was refitted with four CVI Model TM-1200 Re-Entrant Cryopumps, each of which is surrounded by a liquid nitrogen baffle. These cryopumps provide a xenon pumping speed measured at 140,000 l/s with a base pressure of less than 2×10^{-7} Torr. Propellant flow was controlled by two MKS Model 1100 Flow Controllers.

The P5 was positioned on a probe table, which allowed two degrees of freedom over about a meter in each direction. The two translation stages were controlled and monitored via a computer. Resolution was on the order of 0.025 cm for both stages.

Laser and Optics

An argon-ion pumped Coherent dye laser (899-29 model) was used with Rhodamine-6G dye. Typical power was 0.25 W at 605 nm. The laser wavelength was scanned over a 0.01 to 0.04 nm range (10 to 30 GHz) in 0.061 pm (50 MHz) increments. The scanning and the synchronized data collection were computer controlled.

Because of the large natural fluorescence at 529 nm, the laser beams were chopped to phase lock the laser induced fluorescence. In order to distinguish velocity components, the downstream, vertical, and lateral beams were chopped at 1300 Hz, 1000 Hz, and 880 Hz respectively. About 10 percent of the lateral beam was split off downstream of the chopper and passed through the center of a hollow cathode in a Hamamatsu opto-galvanic cell with Xe and Ne gases. The voltage applied across the opto-galvanic cell determined the plasma density and temperature: 330 V gave a strong Xe II signal. A Chromex 0.5 m monochromator with a Hamamatsu 928 photomultiplier tube (PMT) collected the fluorescence.

The laser and optics shown schematically in Fig. 1 are located in a controlled atmosphere/low-dust enclosure. The beams are delivered to the LVTF and then to the thruster as shown in Fig. 5. The mirrors and focusing lens were protected from sputtering deposition and erosion by an enclosure with anti-reflection coated windows, while the collection lens was protected by two separate anti-reflection coated windows. The fluorescence from the thruster plume was collected by a 500M Spex monochromator with a Hamamatsu 928 PMT.

Operational amplifier circuits converted the PMT current signals to voltage signals. Lock-in amplifiers then isolated the fluorescence components of these signals. The Coherent 899-29 Autoscan software collected and matched the laser frequency to these signals.

Laser alignment was facilitated by a 0.1 cm diameter steel wire centered on the downstream face of the thruster. The wire was roughly 7.4 cm from the center of the discharge annulus. The laser beam focal volumes were overlaid on the wire. The locations of the laser spots were measured at two locations below the focusing lens, yielding accurate values for the angles α and β.

Each data collection point required four steps:

1. move the thruster to establish the point of interrogation
2. set the laser wavelength to the upper edge of the scan range,
3. take a computer-controlled scan of the three thruster LIF signals over a period of several minutes, and
4. take a second, shorter scan of the reference cell signal.

Results

The LIF signal strength was optimized at most points of interrogation. A record of the amplifier settings provided a rough indication of the relative

Table 1 P5 operating conditions.

Condition	Disc. Voltage (V)	Disc. Current (A)	Discharge Flow Rate (sccm)	Cathode Flow Rate (sccm)	Facility Pressure (10^{-6} Torr)
1.5 kW	300	5.3	60.0	6.0	5.5
2.5 kW	500	5.3	60.0	6.0	5.5
3.0 kW	300	10.4	114	6.0	8.5

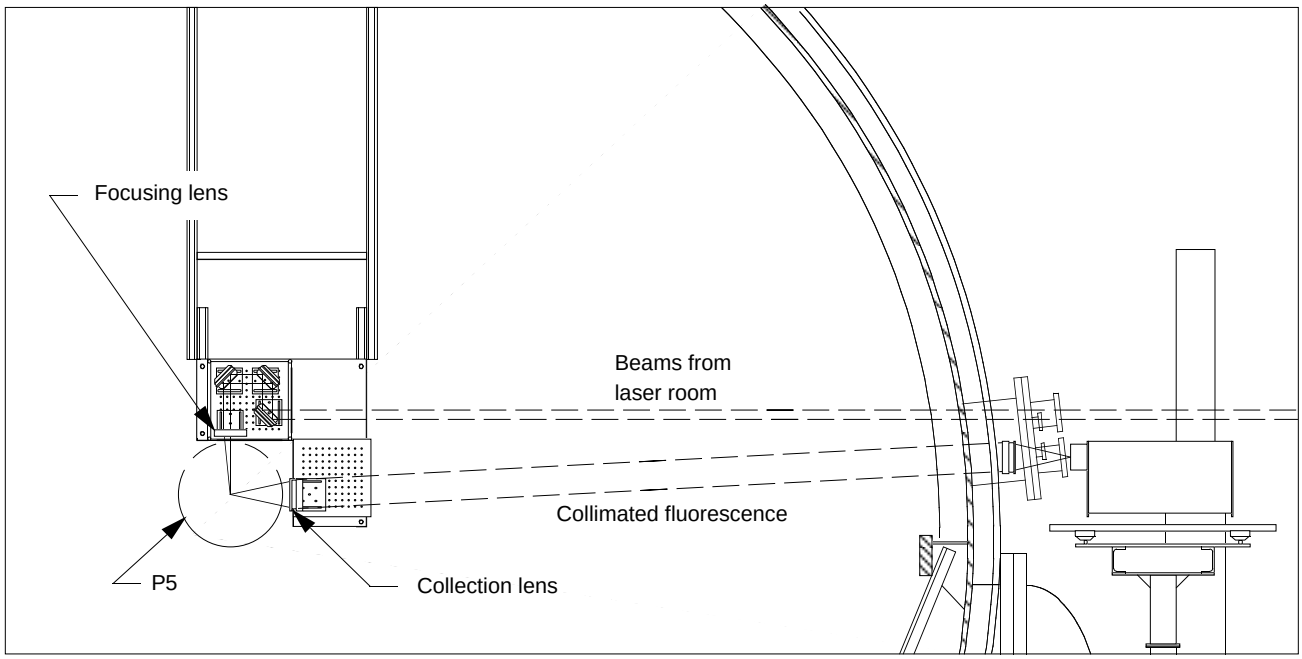

Fig. 5 Laser beam delivery and fluorescence optics schematic.

plasma densities. At the exit of the thruster, the densities were highest in the center of the discharge channel. The density peak shifted to the inner edge of the channel at 10 cm.

Periodically, a polarizer was used to vary the power of the laser beam upstream of the first beam splitter as a check for saturation and power broadening. No saturation or power broadening was observed.

Near-field

Two sets of near-field data were taken during 1.5 kW operation. Two-beam data were collected at 0.1, 0.65, 1.0 and 10. cm. Three-beam data were taken at 0.5, 1.0 and 10. cm. Differences in the data at 1.0 and 10. cm were used to estimate the uncertainty in the measurements of velocity and temperature. This analysis indicated a ten percent error in velocity and a twenty percent error in temperature. The reference cell removed wavelength-related uncertainty, and the angles of the interrogating beams were measured to within one percent. The most likely source of error was the curve fitting used in the data reduction, which is fairly sensitive to noise in the recorded spectral lines. The uncertainties are reflected by error bars in the data presentation below. Data were also taken over the same matrix at the 3 kW operating condition, but only at 1 cm during 2.5 kW operation.

Figures 6 and 7 show typical sets of near-field data for 1.5 kW and 3 kW operation. These figures show trends typical of all near-field data. Note that the data is presented in terms of detuning frequency, facilitating the use of Eqn. 1. A negative frequency shift implies a Doppler shift in the opposite direction to the laser; *i.e*, downstream for the axial component, inwards for the radial component, and upwards for the azimuthal component. Fits used to find the Doppler shift and the temperature of each component are given as dotted lines.

Figure 8 shows the axial velocity profiles for the 1.5 kW case. The velocities are fairly uniform across the discharge, and there is a distinct acceleration of the ions over the first 10 cm. Speeds increase on average from 11000 m/s at 0.1 cm to 16000 m/s at 10 cm. This is shown more clearly in Fig. 9, which shows the same data in terms of energy. Note that the energies are significantly below the discharge voltage (300 V). The axial velocity increased towards the center of the thruster in 2.5 kW operation. The speeds varied from 19,200 m/s to 24,000 m/s.

Figures 10 and 11 show similar trends in axial ve-

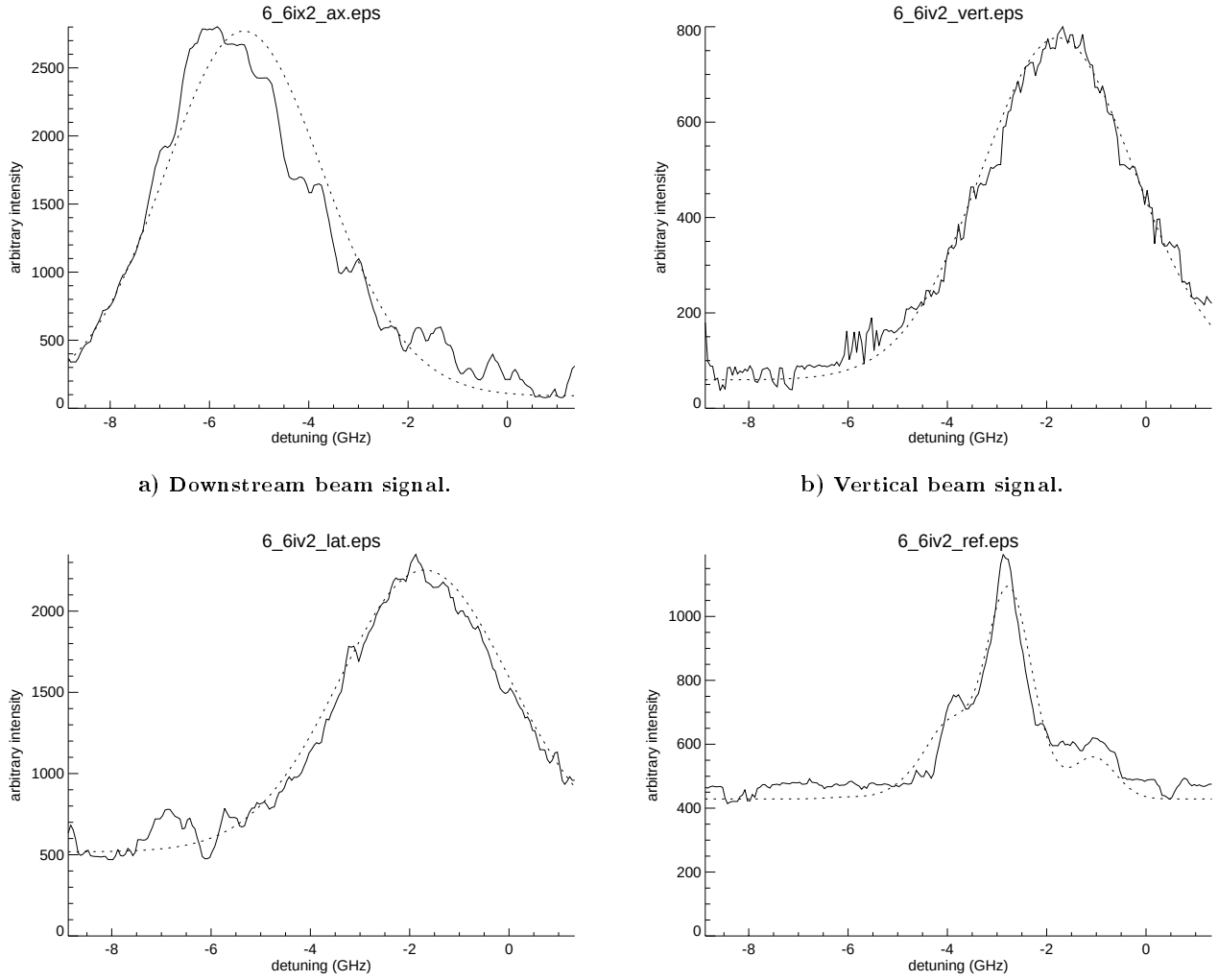

a) Downstream beam signal.

b) Vertical beam signal.

c) Lateral beam signal.

d) Reference cell signal.

Fig. 6 Typical near-field data for 1.5 kW operation.

locity and axial energy for the 3 kW case. Note that the speeds are slightly higher in the 3 kW case. On average, the speed increases from 13000 m/s to 17000 m/s. The increase may result from an increase in the current to the inner magnet from 3 A to 4 A.

Figures 12 and 13 show radial velocity profiles for the 1.5 and 3.0 kW cases. Note that the radial velocity increased with increasing power. Positive velocities are towards the thruster centerline. As might be expected, the divergence is greater near the sides of the channel and minimized along its centerline; however, the velocities are largely independent of axial position. Figures 14 and 15 give vector plots of the in-plane velocities of the ions emitted in the 1.5 and 3.0 kW cases respectively.

Figures 16 and 17 show the temperatures associated with the axial velocities. There was a slight increase in temperature with axial position. All three velocity components had similar temperatures at a given point of interrogation. The temperatures generally fell in the 1 to 2 eV range. The temperatures observed during 2.5 kW operation were comparable.

The azimuthal velocity appeared to be roughly independent of position. The azimuthal velocities were roughly 750 m/s for the 1.5 kW case and 1100 m/s at 3.0 kW. The rotation was clockwise in both cases.

Far-field

Data were also taken along the centerline of the thruster 10, 20, 30, 40, and 50 cm downstream. Strong fluorescence was detected at each of these locations, but the signal at 10 cm was the weakest. The range of axial locations was limited to within 50 cm by the experimental setup. These data were taken with only two beams: downstream and vertical.

Figure 18 shows the data taken at the various axial positions. Note that at 20 cm (Fig. 18a) there are three distinct populations: one shifted well above the reference datum, one below, and a third (much weaker) population shifted slightly above the datum. As the axial distance increases, the side peaks tend to merge towards the center. The center distribution is simultaneously narrowing and increasing in intensity.

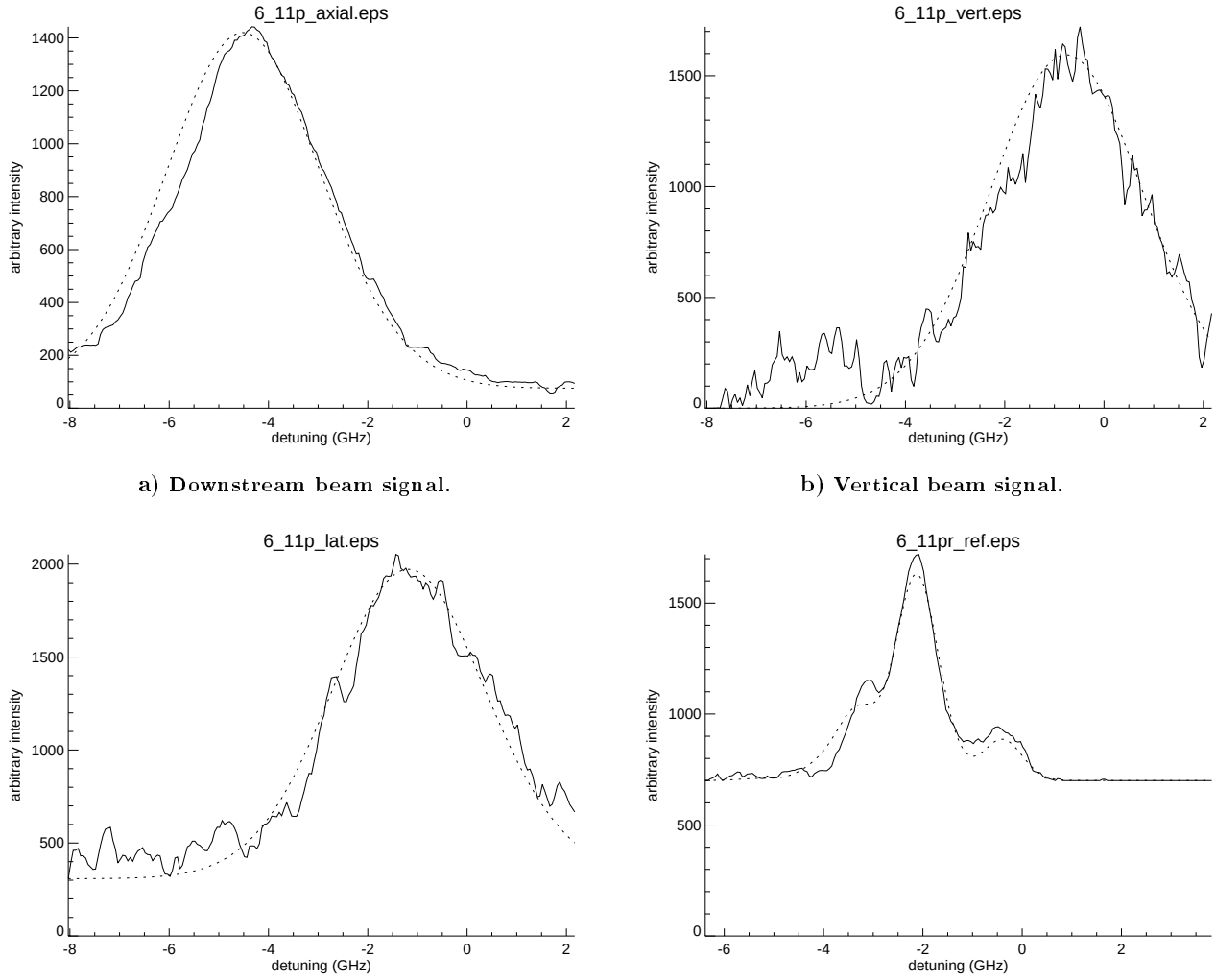

a) Downstream beam signal. **b) Vertical beam signal.**

c) Lateral beam signal. **d) Reference cell signal.**

Fig. 7 Typical near-field data for 3.0 kW operation.

Between 40 and 50 cm, little variation is apparent.

The complex structure of the far-field data precludes accurate modeling with the current model. However, the shifts of the side peaks appears to correspond to the near-field radial velocities, with temperatures on the order of an eV. Each of the axial peaks appears to be shifted by an amount corresponding to the near-field axial velocities. Note that each of the distributions shows roughly the same axial shift. The center distribution appears to have roughly an order of magnitude higher temperature than the side distributions, *i.e.* 10-100 eV. The structure also indicates a significant low-energy tail extending towards the reference cell signal on each of the side distributions.

Discussion

Near-field

The I_{sp} of the P5 has been measured to be about 1500 s in 1.5 kW operation. Accounting for the cathode flow rate, axial velocities on the order of 18,000 m/s were expected. Previous LIF velocity measurements in the 300 V, 4.5 A plume of the SPT-100 Hall thruster indicated an average speed of 15,600 m/s at 1.1 cm downstream.[2] This average is consistent with the speeds measured by 2-beam LIF at the 1.5 kW operating condition, but is somewhat higher than that associated with the 3-beam technique. More confidence is placed in the 2-beam data for this case, because there was a complication in the data reduction of the 3-beam data: the downstream and the vertical beams were scanned subsequently (not simultaneously) to each other in early 3-beam LIF. This complication was removed during 3.0 kW operation, during which all 3 interrogating beams were scanned simultaneously.

The SPT-100 data also indicated a roughly constant azimuthal velocity. The counterclockwise orientation was consistent with the magnetic field orientation of the P5. However, in Manzella's study, there were significant differences between the axial and azimuthal temperatures.

An increase in ion speeds with discharge current at a constant discharge voltage was also observed in a

Stanford, low-power Hall thruster operation.[14] The acceleration region, however, appeared to have roughly a 100 V potential fall in both 1.5 kW and 3.0 kW operation.

Figure 19 shows an MBMS energy spectrum taken 10 cm downstream of the center of the discharge channel during 1.5 kW operation.[3] The peak energy was measured at 260 V with respect to ground. Note that there was also a weaker (1:8) peak at 350 V. The peak energy measured by LIF was about 210 V (roughly 230 V with respect to ground). No second distribution was detected, but the data is sufficiently noisy that a much weaker signal is not precluded at velocities roughly corresponding to 350 V. This second distribution would appear in the high energy wing of the data shown in Fig. 6. The temperature from the LIF scan is much narrower than that from the MBMS data. The reason for this is unclear, but may be due to the divergence of the beam or the presence of multiply charged xenon ions. Both would broaden the MBMS data.

The axial temperatures and azimuthal velocities in this study are in good agreement with near-field LIF on another Hall thruster.[1] However, in that study the temperatures varied significantly between axial and azimuthal components.

The presence of an acceleration region downstream of the thruster agrees with previous LIF data[14] and with recent probe measurements.[15] This region appears to extend beyond 10 cm from the exit plane.

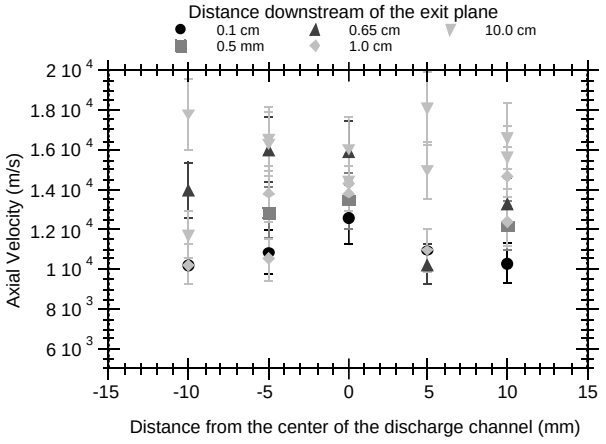

Fig. 8 Axial velocity profiles for 1.5 kW operation.

Far-field

The crossing of the radial components along the centerline of the thruster appears to build the spike observed during operation. Whether the ions are actually colliding is unclear. The glow associated with the spoke would tend to support collisions, but the ion velocities can be redirected via collisionless interactions.

As axial distance increased, narrowing of the global distribution coincided with a decrease in radial velocity. The qualitatively wide distribution in the center

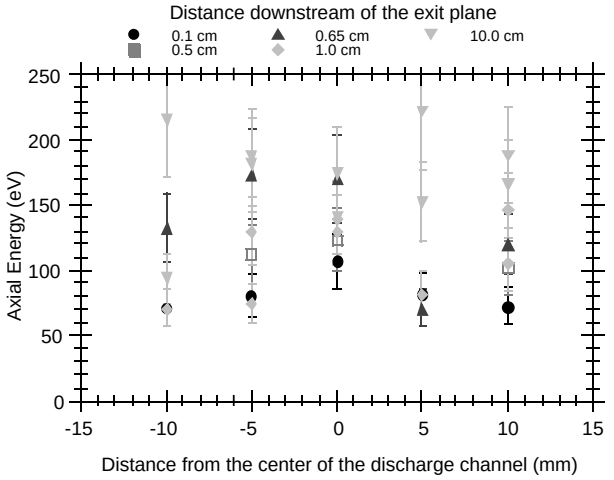

Fig. 9 Peak energy profiles for 1.5 kW operation.

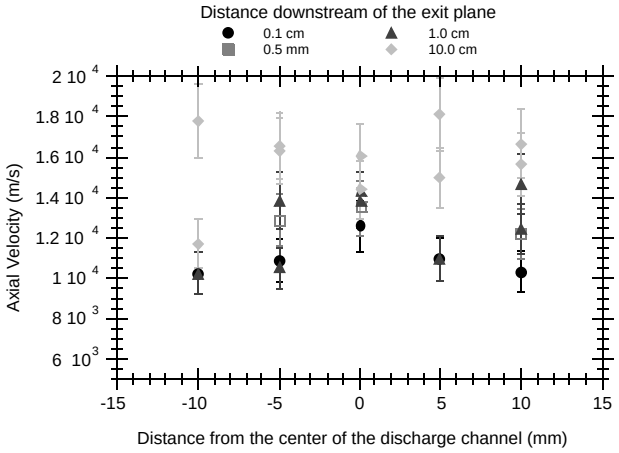

Fig. 10 Axial velocity profiles for 3.0 kW operation.

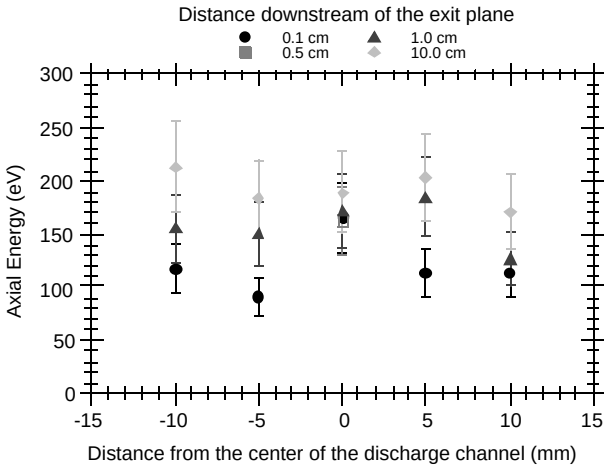

Fig. 11 Peak energy profiles for 3.0 kW operation.

of the global distribution is not visible in the data at 50 cm (Fig. 18d). However, the center distribution may still be present, but masked within the complex structure. This broader distribution (caused by cross-velocities) may be what has been measured by probes in the far-field. The 20 eV distribution observed by

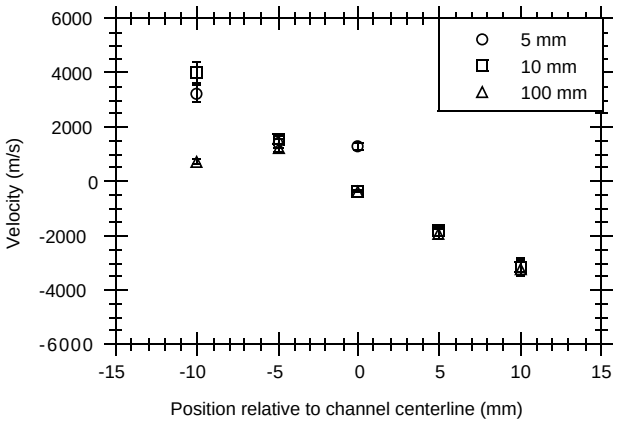

Fig. 12 Radial velocity profiles for 1.5 kW operation.

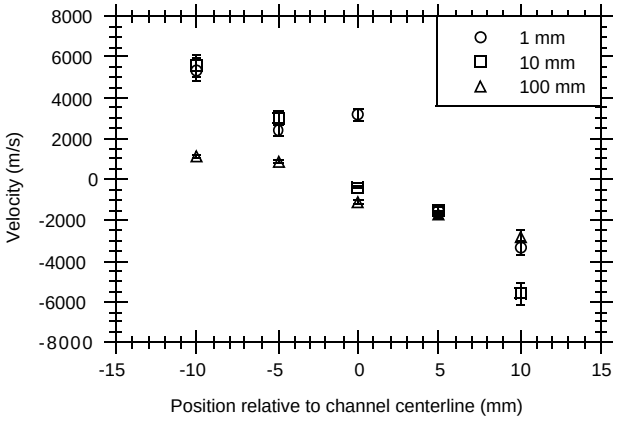

Fig. 13 Radial velocity profiles for 3.0 kW operation.

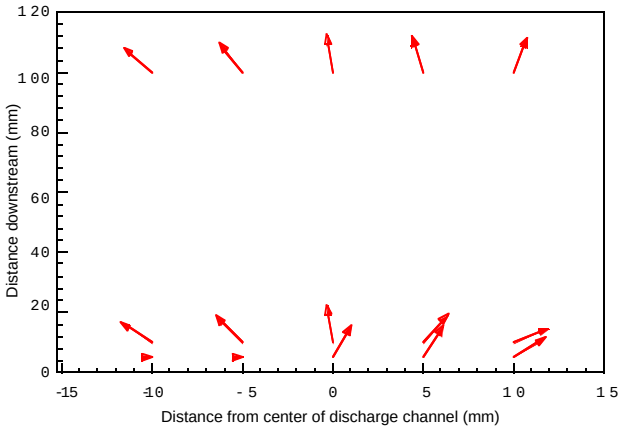

Fig. 14 Vector plot of the 1.5 kW velocities.

MBMS measurements at 10 cm is also consistent with this phenomenological explanation. More data taken off the thruster centerline and better modeling would be required to verify this.

Conclusions

Three-beam LIF has been demonstrated as a viable diagnostic technique for Hall thruster plume velocity measurements. Simultaneous measurement of all three velocity components was achieved. While measured

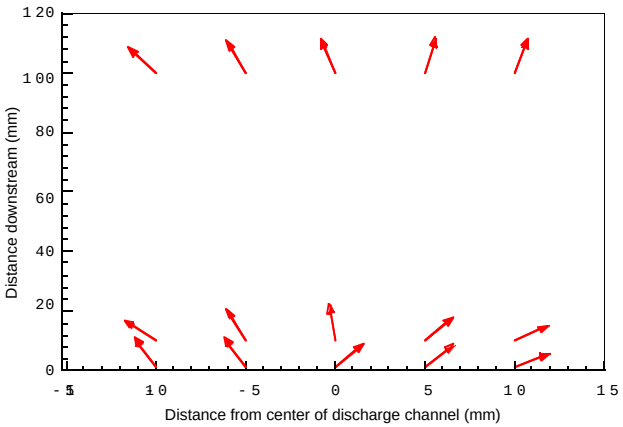

Fig. 15 Vector plot of the 3.0 kW velocities.

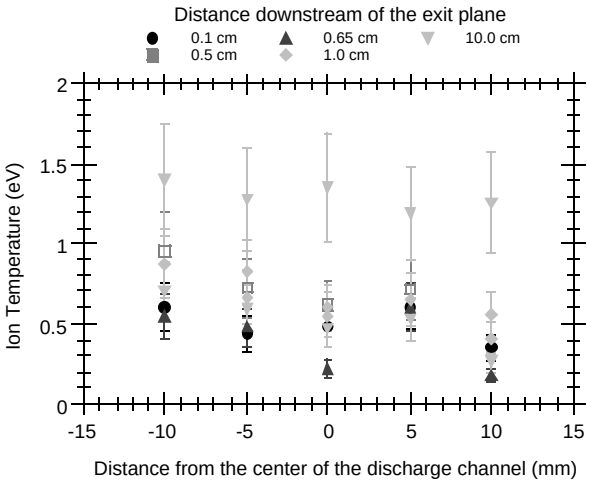

Fig. 16 Ion temperature profiles for 1.5 kW operation.

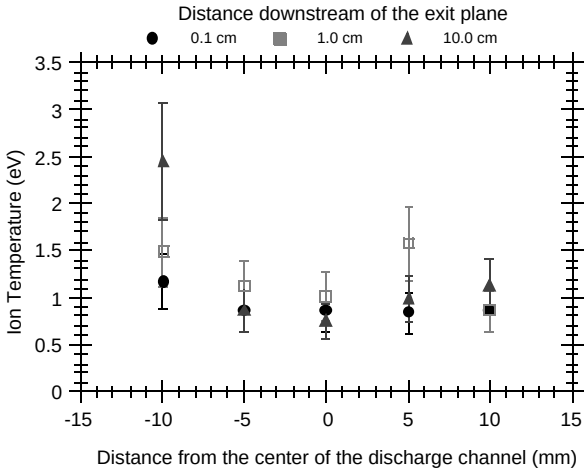

Fig. 17 Ion temperature profiles for 3.0 kW operation.

speeds were lower than those predicted by MBMS measurements, they are not inconsistent with previous LIF measurements. Repeated measurements will be performed to statistically quantify the uncertainty.

An acceleration region was observed extending several centimeters (>10 cm) downstream of the P5 exit

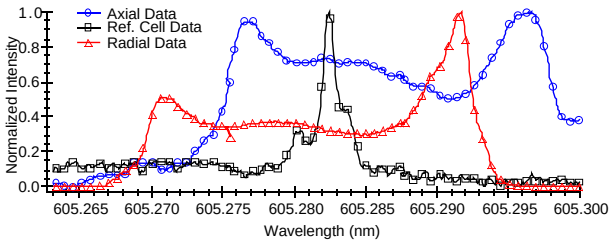

a) 20 cm downstream.

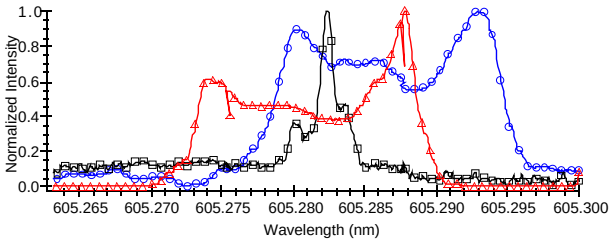

b) 30 cm downstream.

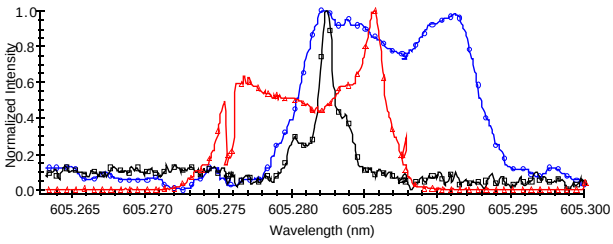

c) 40 cm downstream.

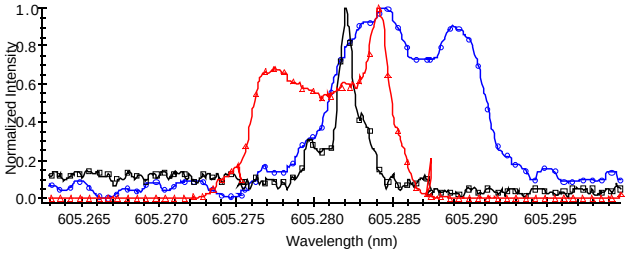

d) 50 cm downstream.

Fig. 18 Far-field data taken along the P5 centerline.

plane. The temperatures of the three velocity components were roughly equal and constant. Both of these support the hypothesis that ionization takes place largely upstream of the exit plane and that there is a distributed acceleration region downstream of the exit plane.

LIF was demonstrated to be of value in the far-field as well as in the near-field The divergence in the near-filed region was roughly independent of axial position and gave rise to a complex velocity distribution along the thruster centerline. The more-or-less axial component of this distribution has a wide half-width, which may account for the widths observed using physical probes. Future investigations will explore this phenomenon more fully.

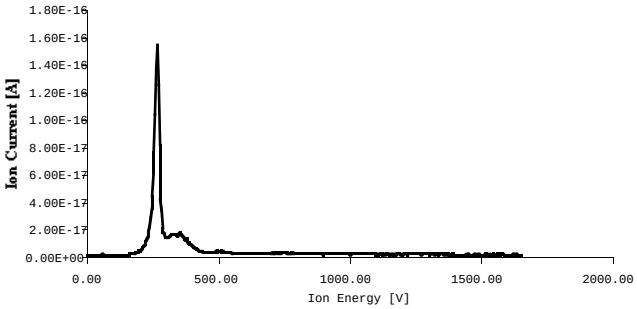

Fig. 19 Ion energy distribution measured by MBMS.

Acknowledgments

This work was made possible by the continuing support of NASA John Glenn Research Center at Lewis Field and the personnel associated with the On-Board Propulsion Branch. The research has been carried out under NASA Grants NAG 31572 and NGT-3-52311. The authors would also like to thank the other students in the PEPL group for their assistance and support.

References

[1]King, L. B. et al., "Transport-property Measurements in the Plume of an SPT-100 Hall Thruster," *AIAA Journal of Propulsion and Power*, Vol. 14, No. 3, March 1998, pp. 327–335.

[2]Manzella, D. H., "Stationary Plasma Thruster Ion Velocity Distribution," *Proceedings of the 30th Joint Propulsion Conference*, AIAA-94-3141, June 1994.

[3]Gulczinski, F. S., Hofer, R. R., and Gallimore, A. D., "Near-Field Ion Energy and Species Measurements of a 5 kW Laboratory Hall Thruster," *Proceedings of the 35th Joint Propulsion Conference*, AIAA-99-2430, June 1999.

[4]Domonkos, M. T. et al., "Very Near-field Plume Investigation of the D-55," *Proceedings of the 33rd Joint Propulsion Conference*, AIAA-97-3062, July 1997.

[5]Keefer, D. et al., "Multiplexed Laser Induced Fluorescence and Non-Equilibrium Processes in Arcjets," *Proceedings of the 25the Plasmadynamics and Lasers Conference*, AIAA-94-2656, July 1992.

[6]Kopfermann, H., *Nuclear Moments*, Academic Press, 1958.

[7]Candler, C., *Atomic Spectra and the Vector Model*, Van Nostrand, 1964.

[8]Bingham, C. et al., "Collinear fast-beam laser spectroscopy experiment: measurement of hyperfine structure and isotope shifts in Xe II," *Nuclear Instruments and Methods*, Vol. 202, No. 147, May 1982.

[9]Verdeyen, J., *Laser Electronics*, Prentice-Hall, 1995.

[10]Haas, J. et al., "Performance Characteristics of a 5 kW Laboratory Hall Thruster," *Proceedings of the 34th Joint Propulsion Conference*, AIAA 98-3503, July 1998.

[11]Arkhipov, B. et al., "Extending the Range of SPT Operation: Development status of 300 and 4500 W Thrusters," *Proceedings of the 32nd Joint Propulsion Conference*, AIAA 96-2708, July 1996.

[12]Garner, C. E. et al., "'Evaluation of a 4.5 kW D-100 Thruster with Anode Layer," *Proceedings of the 32nd Joint Propulsion Conference*, AIAA 96-2967, July 1996.

[13]Petrosov, V. A. et al., "Investigation 4.5 kW High Efficiency Hall Type T-160 Electric Thruster," *Proceedings of the 24th International Electric Propulsion Conference*, IEPC 95-03, Sept. 1995.

[14]Cedolin, R. et al., "Laser-Induced Fluorescence Study of a Xenon Hall Thruster," *Proceedings of the 33rd Joint Propulsion Conference*, AIAA-97-3053, July 1997.

[15]Haas, J. M., Hofer, R. R., and Gallimore, A. D., "Hall Thruster Discharge Chamber Plasma Characterization using a High Speed Axial Reciprocating Electrostatic Probe," *Proceedings of the 35th Joint Propulsion Conference*, AIAA-99-2426, June 1999.